Hot Electron Injection from Graphene Quantum Dots to TiO₂
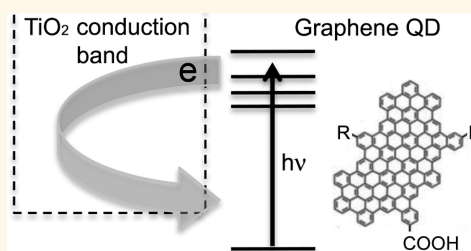
Kenrick J. Williams,[†] Cory A. Nelson,[†,‡] Xin Yan,[§] Liang-Shi Li,[§] and Xiaoyang Zhu[†,‡,*]

[†]Department of Chemistry & Biochemistry, University of Texas, Austin, Texas 78712, United States, [‡]Department of Chemistry, Columbia University, New York, New York 10027, United States, and [§]Department of Chemistry, Indiana University, Bloomington, Indiana 47405, United States

ABSTRACT   The Shockley—Queisser limit is the maximum power conversion efficiency of a conventional solar cell based on a single semiconductor junction. One approach to exceed this limit is to harvest hot electrons/holes that have achieved quasi-equilibrium in the light absorbing material with electronic temperatures higher than the phonon temperature. We argue that graphene based materials are viable candidates for hot carrier chromophores. Here we probe hot electron injection and charge recombination dynamics for graphene quantum dots (QDs, each containing 48 fused benzene rings) anchored to the TiO₂(110) surface *via* carboxyl linkers. We find ultrafast electron injection from photoexcited graphene QDs to the TiO₂ conduction band with time constant $\tau_i < 15$ fs and charge recombination dynamics characterized by a fast channel ($\tau_{r1} = 80-130$ fs) and a slow one ($\tau_{r2} = 0.5-2$ ps). The fast decay channel is attributed to the prompt recombination of the bound electron—hole pair across the interface. The slow channel depends strongly on excitation photon energy or sample temperature and can be explained by a "boomerang" mechanism, in which hot electrons are injected into bulk TiO₂, cooled down due to electron—phonon scattering, drifted back to the interface under the transient electric field, and recombine with the hole on graphene QDs. We discuss feasibilities of implementing the hot carrier solar cell using graphene nanomaterials.

KEYWORDS: hot electrons · graphene quantum dots · charge transfer · hot carrier solar cells

The Shockley—Queisser limit[1] (~31%) is dictated by two energy loss mechanisms: (i) the chromophore does not absorb photons with energy below the bandgap; (ii) photons with energy exceeding the bandgap creates "hot" electrons and holes whose excess energy is quickly lost before they are captured, as shown in Figure 1a. One proposal to exceed the Shockley-Queisser limit is to capture the hot electrons and holes before they are cooled to the band-edges, and the theoretical solar-to-electric power conversion efficiency of such a hot carrier solar cell can be as high as 66%.[2,3] However, before this exciting concept can be realized, two stringent conditions must be met, as illustrated in Figure 1b. The first condition concerns hot carrier interactions. The hot electrons (holes) need to reach a quasi-equilibrium approximated by an electron (hole) temperature higher than that of the lattice or the surrounding environment.[2,3] This requires a sufficiently high density of hot carriers within a scattering volume and hot carrier cooling by phonon scattering must be slower than carrier—carrier scattering. To understand the need for hot

electron (hole) scattering, consider a photoexcited electron above the conduction band minimum but below the hot electron extraction level. In the conventional picture, this conduction band electron cannot be extracted. However, in the presence of hot electron scattering, the electron with energy below the hot electron extraction level can scatter with one at higher energy to bring both into resonance with the extraction level, thus increasing the photocurrent. The second condition is on hot carrier extraction. Electrons (holes) with energy in excess of the Fermi level of the electron (hole) conductor will be lost after transfer. To minimize energy loss within the electron (hole) conductor, the hot electrons (holes) should ideally be extracted in a narrow energy window near the Fermi level. This requires the presence of interfacial electronic energy levels ("band-pass" filters), for example, from molecular orbitals, for hot carrier transfer.

Semiconductor nanocrystals or quantum dots (QDs) have been explored as light absorbers for high-efficiency solar energy conversion,[4−6] including as chromophores for
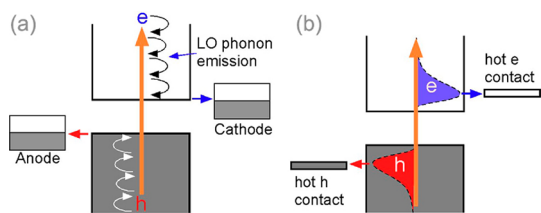
Figure 1. Schematic illustration of a conventional solar cell (a) and a hot-carrier solar cell (b).

hot electron injection.[7] However, there are fundamental limitations in using semiconductor QDs for a hot carrier solar cell. This is because achieving quasi-equilibrium of hot carriers requires not only long hot carrier lifetime, but also sufficient excitation density and electronic delocalization to ensure inter-electron (or hole) scattering before they are extracted or cooled down by phonons. This is exceptionally challenging because the perceived advantage of semiconductor QDs in slowing down hot carrier cooling *via* the so-called "phonon bottleneck" effect[8,9] does not exist for highly excited electron/holes that behave essentially bulk-like.[10,11] The phonon bottleneck has been found only for the lowest excited levels in QDs with exceptionally well-engineered interfaces[12] but absent in most other cases.[13−19] Further more, ensuring carrier−carrier scattering to reach quasi-equilibrium requires the presence of more than one excitation within the limited lifetime of a hot carrier, but the low photon flux from solar radiation presents a formidable challenge. The solar radiation on the surface of the earth is ~ 1 kW/m^2, corresponding to a spectrally integrated photon flux of $\sim 10^{-8}$ photons nm^{-2} ps^{-1} in the broad range from near-IR to UV. Given a typical photoabsorption cross section of 1 nm^2 for a QD, even with a hot electron lifetime of 100 ps, one would need a solar concentration of $>10^6$ to obtain more than one excitation per QD. This is the *photon flux challenge*. Meeting this challenge would necessitate sufficient electronic delocalization and high carrier velocity to ensure scattering at low densities. In principle, the formation of hot carrier mini-bands with large bandwidth in QD solids may provide the electronic delocalization, but the inevitable presence of intrinsic disorder makes this unlikely.

Here we explore graphene nanomaterials[20] as hot carrier chromophores, particularly bottom up synthesized and solution processable graphene-like molecules that have been called large polycyclic aromatic hydrocarbons[21] or colloidal graphene QDs,[22] with high extinction coefficients and tunable optical gaps. Li and co-workers reported hot electron lifetimes in graphene GDs as long as 10^2 ps,[23] which is reminiscent of the "phonon bottleneck", and demonstrated their applications as light absorbers in dye-sensitized solar cells.[22] As the size of these graphene QDs (now typically consisting of ≤ 100 fused benzene rings) increases further, some of their physical properties may start to approach those of

graphene. Particularly desirable properties of graphene for hot carrier solar cells include the highly delocalized nature of excited electrons/holes with exceptionally high velocity of 10^6 m s^{-1}, inefficient electron−phonon scattering, but exceptionally efficient intra-band electron−electron (hole−hole) scattering.[24,25] The latter results from the linear dispersion which guarantees the conservation of both energy and momentum simultaneously during carrier−carrier scattering. These properties lead to transient equilibration of hot electrons (holes) on the ultrafast time scale (≤ 100 fs), which is 1 order of magnitude shorter than the hot carrier cooling time.[26−29] The efficient equilibration of hot electrons (holes) in optically excited[30] or electrically biased graphene[31] has been shown to yield light emission characteristic of blackbody radiation at high electronic temperatures (*e.g.*, ≥ 1500 K). Hot carrier equilibration is even possible under solar radiation as illustrated in the following. With a realistic solar concentration of 10^2, the solar photon flux is 10^{-6} photons nm^{-2} ps^{-1} in the IR-UV range. For a graphene flake of $\sim \mu$m^2, the optical absorption cross-section and carrier scattering area are of the same order. There are 10^2 hot carriers in this scattering volume (area) within the hot carrier lifetime of ~ 100 ps. Hot carrier scattering and equilibrium is possible at such a density. Thus, we can meet the photon flux challenge using graphene based materials.

In this report, we demonstrate the feasibility of hot electron harvesting from graphene QDs chemically anchored in the monolayer region to a single crystal TiO$_2$(110) surface. Using time-resolved second harmonic generation, we find ultrafast electron injection from photoexcited graphene QDs to the TiO$_2$ conduction band with time constant <15 fs at all exciton photon energies and sample temperatures used. In contrast to electron injection, charge recombination depends strongly on excitation photon energy or sample temperature and can be explained by hot electron injection and cold polaron recombination.

RESULTS AND DISCUSSION

We use a graphene QD molecule (referred to as C132A) consisting of a 132-C graphene core (48 fused benzene rings), functionalized with two 2,4,6-trialkyl-substituted phenyl groups for solubility and a carboxylic acid group for attachment to TiO$_2$ surface (Figure 2a).[22] Figure 2b shows an absorption spectrum of C132A solution in chloroform. As detailed before,[23] the main absorption peak in the visible region consists of four electronic transitions (S1−4), with the most intense peak at S$_3$. Adsorption of C132A molecules from chloroform solution onto a clean single crystal TiO$_2$(110) surface results in two-dimensional islands of height ~ 4 nm (see height histogram in Figure 2d), which corresponds to the C132A molecules adopting the standing-up conformation with the −COOH group forming bidentate linkages to the TiO$_2$ surface and
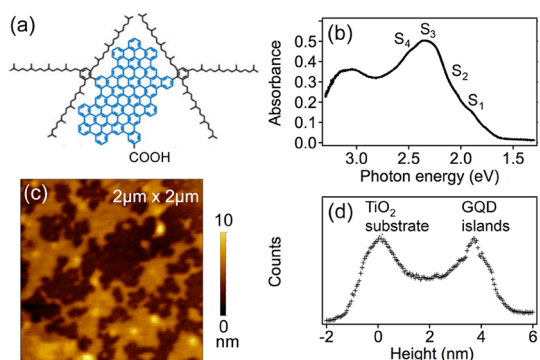
Figure 2. (a) Structure of the C132A graphene QD molecule; (b) optical absorption spectrum of C132A in chloroform solution. Note the approximate positions of the excitonic states; (c) 2 μm × 2 μm AFM image of a C132A submonolayer assembled on TiO$_2$ (110); (d) histogram of heights from the AFM image in panel c.
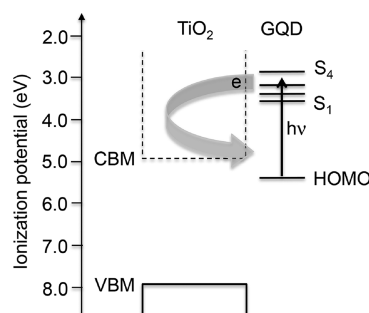

Figure 3. Energy level diagram of the C132A molecule (GQD) on the TiO$_2$ surfaces. VBM, valence band maximum; CBM, conduction band minimum. See text for a discussion on the approximate position of the conduction band (dashed box). The thick arrow illustrates hot electron injection into TiO$_2$ conduction, cooling and localization of the electron into an electron polaron, and recombination across the interface of the electron polaron with the hole on a GQD.
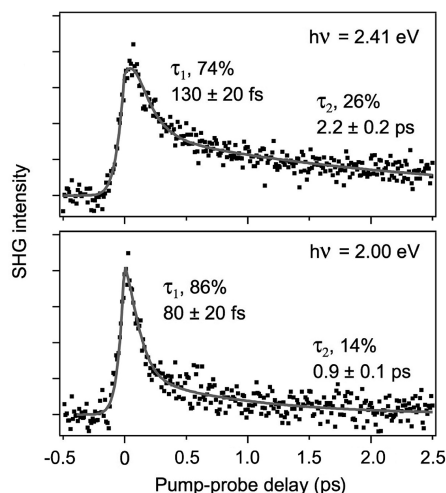
with packing density as high as one QD per 2 nm^2.[32] By integrating the histogram data in Figure 2d, we determined the surface coverage to be 0.5 monolayer (ML). Photoinduced electron transfer from graphene QDs to TiO$_2$ is known to occur from solar cell measurement.[22] The workfunction of TiO$_2$(110) is 5.2 eV and the conduction band minimum (CBM) lies 0.3 eV above the Fermi level;[33,7] the CBM lies at 4.9 eV below the vacuum level. The threshold ionization potential of C132A is 5.3 eV (below vacuum level).[34] In the absence of significant surface dipole formation upon the assembly of C132A on TiO$_2$(110), the threshold optical gap of ~1.6 eV (Figure 2b) puts excitonic states at ≥1.2 eV above the CBM of TiO$_2$. Thus, we expect hot electron injection significantly above the TiO$_2$ CBM from photoexcited C132A. Figure 3 shows an energy level diagram of the graphene QD/TiO$_2$ interface. We use ionization potential (referenced to the vacuum level) to include the quasi-particle excitonic states in C132A and the TiO$_2$ valence band on the same scale. Note that the conduction band of TiO$_2$ (dashed box) is included here as an approximation. The ionization potential of an electron in the conduction band is higher than the single-electron transport energy (i.e., vertical electron affinity) by the electron polaron binding energy, which is ~0.3 eV in TiO$_2$.[35]

To determine the dynamics of charge transfer from photoexcited graphene QDs to TiO$_2$, we apply the experimental technique of femtosecond time-resolved second harmonic generation (TR-SHG), particularly electric field induced SHG (EFISH).[36−38] EFISH is a four-wave mixing process in which two optical fields of frequency ω mix with a quasi-DC field to give a resultant signal at frequency 2ω. In this approach, the pump-induced change in the SHG signal measures the transient (quasi-DC) electric field induced by interfacial charge transfer and is directly proportional to the number of separated charge, as we recently demonstrate for photoinduced electron transfer at the PbSe QDs/TiO$_2$ and an

Figure 4. TR-SHG spectra (dots) for 0.5 ML C132A/TiO$_2$(110) at 300 K and pump photon energies of hν = 2.41 eV (upper) and 2.00 eV (lower). The solid curves are biexponential fits with fitting parameters indicated on each spectrum. The error range represents statistical variations from repeated fits. The probe photon energy for SHG is at 1.53 eV, with second harmonic detected at 3.06 eV.

organic donor/acceptor interface.[7,39] Figure 4 shows TR-SHG spectra at two pump photon energies, hν = 2.00 and 2.41 eV, corresponding to the excitation of the GQD S$_1$−S$_2$ and S$_3$ transitions, respectively. In both cases, we see an ultrafast rise in the SHG signal (and thus interfacial electric field). Within the time resolution given by the pump−probe cross correlation (~60 fs), we are not able to resolve the rise time. We conclude that photoinduced electron transfer from the graphene QD to the TiO$_2$ conduction band occurs on the ultrashort time scale of <15 fs. We attribute the ultrafast electron injection to strong electronic coupling between the graphene QD and the TiO$_2$ conduction band through the carboxylate linker. Ultrafast photoinduced electron injection has also been observed before for other dye molecules anchored to the TiO$_2$ surface via the carboxylate linker.[40] Note that at the excitation photon

energies used here (hν = 2.00 and 2.41 eV), TiO_2 (bandgap ~3.0 eV) is not optically excited.

As negative control, we find no measurable electron injection (pump-induced SHG) for the C132 GQDs without the carboxyl anchoring groups but physically adsorbed on the TiO_2 surface. Yan et al. showed that, when these physisorbed GQSs were used as dye molecules in dye-sensitized solar cells (DSSCs) based on nanocrystalline TiO_2, photovoltaic action was observed.[22] However, the measured photocurrent was nearly two-orders of magnitude lower than those of state-of-the-art DSSCs based on chemically anchored ruthenium complexes. The very low photocurrent of the DSSC with physisorbed GQDs was attributed to slow electron injection from GQDs to TiO_2 in the absence of chemical anchors. Supporting this interpretation, Yan et al. found more recently that the photocurrent was increased by more than 1 order of magnitude when the GQD molecules were chemically anchored to the TiO_2 surface through carboxyl functional groups.[41] Compared to the ultrafast electron injection observed in Figure 4 for chemically anchored GQDs, a slow electron injection process for physisorbed GQDs is expected to spread out the EFISH signal over a large time window, thus, diminishing TR-SHG signal to a level below our detection limit.

We now focus on the charge recombination rates that are dependent on excitation photon energy. Since the experiment does not involve a complete circuit for photoelectron extraction, each excited electron injected into the conduction band of TiO_2 returns to the interface and recombines with the positive hole on a graphene QD molecule. This recombination process is reflected in the decay of the transient interfacial electric field and, thus, SHG signal. The SHG signal decay rate is clearly slower at the higher excitation photon energy. In each spectrum, the decay process is not a single exponential. The gray curves in Figure 4 show biexponential fits that give the indicated populations and decay time constants. At hν = 2.00 eV, charge recombination dynamics can be described by a major channel with $\tau_1 = 80 \pm 20$ fs (86%, relative population) and a minor channel with $\tau_2 = 0.9 \pm 0.1$ ps (14%). Both channels slow down when hν is increased to 2.41 eV: $\tau_1 = 130 \pm 20$ fs (74%) and $\tau_2 = 2.2 \pm 0.2$ ps (26%). We take the inverse dependence of charge recombination rate on excitation photon energy as evidence for hot electron injection from graphene QDs to the TiO_2 conduction band. At higher hν, the excited electron in the GQD possesses higher kinetic energy (above the TiO_2 CBM) and is, thus, injected deeper into TiO_2 from the interface, before being cooled down and localized as an electron polaron.[42] As a result, the electron polaron further away from the interface takes longer to return to the interface for recombination with the hole. The actual dynamics of electron injection/recombination is complex, as it is under the influence of both the electric field due to the positive hole and hot electron cooling due to
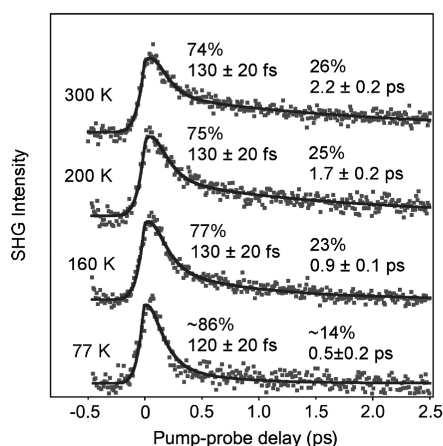

Figure 5. TR-SHG spectra (dots) for 0.5 ML C132A/TiO_2(110) at a pump photon energy of hν = 2.41 eV and the indicated sample temperatures, from bottom to top, T = 77, 160, 200, and 300 K. The solid curves are biexponential fits with fitting parameters indicated on each spectrum. The error range represents statistical variations from repeated fits. The probe photon energy for SHG is at 1.53 eV, with second harmonic detected at 3.06 eV.
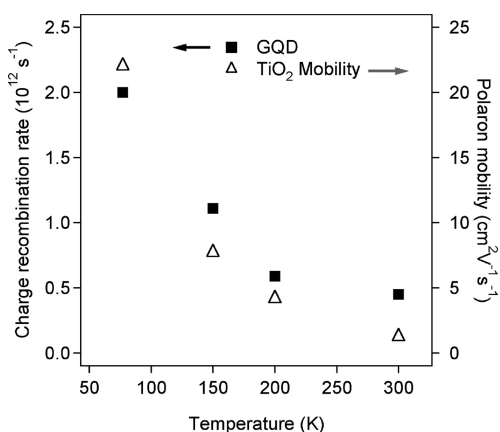

Figure 6. A comparison of the charge recombination rate constants in the slow channel at the C132A/TiO_2(110) interface (solid squares, left axis) with electron polaron mobilities in TiO_2 (open triangles, right axis, ref 42) in the temperature window of 77−300 K.

scattering with phonons in TiO_2. Such a complex dynamic process may explain the multiexponential behavior in recombination dynamics. In a simplified interpretation, the fast recombination channel may be attributed to a nonequilibrium electron population staying in the interface region and recombine promptly, while the slow recombination channel can be due to the thermally equilibrated electron population which has been injected into regions away from the interface, relaxed as electron polarons, and returned to the interface for recombination. Hot electron injection from photoexcited graphene QDs to TiO_2 is also expected as the electron injection time (<15 fs) is much faster than the hot electron cooling time (10^2 ps) within each graphene QD molecule.[23]

Further support for the hot electron injection mechanism can be found in the temperature-dependent

recombination dynamics, as shown in Figure 5 for an excitation photon energy of $h\nu = 2.41$ eV. While the electron injection times (rises in SHG intensity) are too fast to be measured (<15 fs) at all temperatures (77–300 K), the charge recombination rates are clearly temperature dependent. This is most obvious in the time constant of the slow channel which presumably corresponds to hot electrons that have been injected into the bulk TiO$_2$, cooled down by electron–phonon scattering, and returned to the interface as electron polarons for recombination with holes on GQDs. Because the mobility of electron polarons decreases with increasing temperature,[42] the recombination process slows down, from 0.5 ps at 77 K, to 0.9, 1.7, and 2.2 ps when the temperature is increased to 160, 200, and 300 K. This temperature dependence in recombination time is in excellent agreement with the temperature dependence in electron polaron mobility in TiO$_2$, as determined by terahertz spectroscopy[42] and shown in Figure 6. Note that, within experimental uncertainty, the charge recombination time constant for the fast channel ($\tau_1 = 120–130$ fs) is independent of temperature. This further supports the interpretation that the fast recombination channel corresponds to the injected electron staying at the interface, likely bound by the hole in the form of charge transfer exciton across the interface,[43] and promptly recombines.

It is instructive to compare the findings presented here on graphene QDs/TiO$_2$ to previous experiments and theoretical calculations on the PbSe QDs/TiO$_2$ system. For PbSe QDs capped with small molecules (e.g., ethanedithiols), TR-SHG measurements revealed ultrafast hot electron injection from photoexcited QDs to TiO$_2$ with time constant ≤ 30 fs.[7] The interfacial electron injection rates are faster than hot electron cooling rates in both PbSe and graphene QDs,[11,23] in agreement with time-domain ab initio calculations of Prezhdo and co-workers who showed that hot electron injection into the TiO$_2$ conduction band is more competitive than cooling due to electron–phonon scattering in PbSe QDs or in single layer graphene adsorbed on the TiO$_2$ surface.[44,45] Note that for graphene adsorbed parallel to a bulk semiconductor surface, there is a momentum barrier for electron injection. Excited electrons in graphene are near the **K** point in momentum space, while for a typical crystalline semiconductor electron acceptor, such as TiO$_2$, the conduction band minimum is at the $\mathbf{\Gamma}$ point. Interfacial electron transfer must be accompanied by scattering with phonons to compensate for the momentum change (from $k_{\parallel} \approx 1.7$ Å^{-1} near the **K** point in graphene to $k_{\parallel} \approx 0$ near the $\mathbf{\Gamma}$ point in electron acceptor). This momentum requirement is relaxed when at least one of the two materials is in a nanoscale format, such as the graphene QDs used here or colloidal titania nanosheets demonstrated recently in graphene–titania multilayer composites for ultrafast electron transfer.[46]

In contrast to electron injection, charge recombination dynamics at the graphene QDs/TiO$_2$ interface is very different than that at the PbSe QDs/TiO$_2$ interface. In the latter, the fast recombination channel is absent and the recombination process is single exponential, with time constants ~5 times longer than those of the slow channels at the graphene QDs/TiO$_2$ interface. We attribute the difference at the two interfaces to the much larger (more than 1 order of magnitude) dielectric constant of PbSe than that of graphene QDs; the large dielectric constant effectively screens the positive hole, thus preventing the formation of interfacial charge transfer excitons and reducing the magnitude of the transient electric field responsible for the drift of electron polarons back to the interface for recombination. In an actual device, such as the dye-sensitized solar cell, the hole on the graphene QD may be effectively screened by the presence of electrolytes, thus reducing or eliminating the prompt recombination channel attributed to the bound electron–hole pair across the interface. It is desirable to apply the TR-SHG technique to probe charge recombination dynamics for the QDs/TiO$_2$ interface in the presence of electrolytes, but this would be technically very challenging because the addition of another interface significantly complicates the analysis of nonlinear optical responses. Note that the picosecond charge recombination dynamics observed at the GQD/TiO$_2$ interface is faster than (by as much as 1–2 orders of magnitude in some cases) those at other dye/TiO$_2$ interfaces measured previously.[40] We speculate that the difference might be attributed to differences in reorganization energies. A GQD molecule is much more rigid than a conventional dye molecule; as a result, we expect a much larger reorganization energy in the latter and a higher activation energy for back electron transfer from TiO$_2$ to the molecule.

CONLCUSIONS

We establish hot electron injection and charge recombination dynamics for graphene QDs, anchored to the TiO$_2$(110) surface via carboxyl linkers using femtosecond time-resolved second harmonic generation. We find ultrafast electron injection from photoexcited graphene QDs to the TiO$_2$ conduction band with time constant $\tau_i < 15$ fs. Electron–hole recombination is characterized by a fast channel ($\tau_{r1} = 80–130$ fs) and a slow one ($\tau_{r2} = 0.5–2$ ps); the former is attributed to the prompt recombination of the bound electron–hole pair across the interface while the latter depends strongly on excitation photon energy or sample temperature, and can be explained by a "boomerang" mechanism consisting of hot electrons injection and cooled electron-polaron transport and recombination. Given the size of each graphene QD molecule, the photon flux challenge is still not met: it is impossible to have multiple excitations in each molecule under

solar radiation. We need to increase the size of each graphene nanostructure to reach the scales of hundreds of nanometers to micrometer; this may be feasible with graphene flakes or graphene nanoribbons. These graphene structures in the 10^2 nm to μm size range may serve as an ideal hot carrier chromophore, allowing multiple electronic excitations under reasonable solar concentration and ultrafast equilibration of hot electrons (holes) to yield quasi-thermal distributions. With these properties, when combined with the equally important energy-selective transfer of hot electrons and holes to corresponding accepting materials through proper interfacial engineering, as well as dielectric screening to minimize competitive recombination channels, the conceptual sketch in Figure 1b may eventually become an experimental reality.

METHODS

We assembled C132A onto the surface of a rutile TiO_2(110) single crystal surface (MTI Corp). Briefly, we cleaned the TiO_2 surface using the procedure of Parkinson and co-workers (1 M HCl under UV irradiation for 30 min, followed by rinsing with deionized water and acetone).[47] The TiO_2 was submerged in a nearly saturated C132A/chloroform solution in a capped vial and the chloroform was allowed to slowly evaporate in excess of 24 h. We then added enough chloroform to redissolve the precipitated C132A and let chloroform evaporate for 24 h. After repeating this procedure for the third time, we removed the TiO_2 sample from the chloroform solution, rinsed the surface with chloroform and dried it under a stream of nitrogen. This procedure resulted in a submonolayer of surface assembled C132A molecules, as shown by atomic force microscopy (AFM) image in Figure 2c.

For TR-SHG measurements, the C132A/TiO_2(110) sample was mounted in a cryostat evacuated to 10^{-7} Torr with sample temperature controlled by liquid nitrogen cooling and resistive heating. The light for TR-SHG comes from a pulsed Ti-sapphire laser (Coherent, RegA 9050, 250 kHz, $\lambda = 810$ nm), whose output is split into two beams, one as probe, and the other to generate a tunable pump beam (500 − 750 nm) *via* optical parametric amplification. The pump and time-delayed probe laser pulse energy densities on the sample surface are in the range of a few to a few tens of μJ cm^{-2}. Cross-correlation analysis gives pump and probe laser pulse widths of ∼60 fs. The two laser beams are directed at the sample surface noncollinearly (5°), with a 0.26 mm × 0.36 mm elliptical spot on the surface. The plane of incidence is defined by the (110) and the (1$\bar{1}$0) crystalline directions of the rutile TiO_2(110) sample, with incident probe and reflected light 45° from surface normal. The reflected SHG light, almost entirely of p-polarization, is detected with a photomultiplier tube and a gated photon counter. We controlled the pump laser fluence to give an estimated excitation densities of ∼50% of C132A molecules, calculated using a molar absorptivity at 520 nm of $\varepsilon = 1 \times 10^5$ M^{-1} cm^{-1}. Note that there is no pump-induced SHG signal for bare TiO_2(110) surface under otherwise identical experimental conditions.[7]

Conflict of Interest: The authors declare no competing financial interest.

REFERENCES AND NOTES

1. Shockley, W.; Queisser, H. J. Detailed Balance Limit of Efficiency of P−N Junction Solar Cells. *J. Appl. Phys.* **1961**, *32*, 510–519.
2. Ross, R. T.; Nozik, A. J. Efficiency of Hot Carrier Solar Cell Converters. *J. Appl. Phys.* **1982**, *53*, 3813–3818.
3. Wurfel, P. Solar Energy Conversion with Hot Electrons From Impact Ionisation. *Solar Energy Mater. Solar Cells* **1997**, *46*, 43–52.
4. Baxter, J.; Bian, Z.; Chen, G.; Danielson, D.; Dresselhaus, M. S.; Fedorov, A. G.; Fisher, T. S.; Jones, C. W.; Maginn, E.; Kortshagen, U.; *et al.* Nanoscale Design to Enable the Revolution in Renewable Energy. *Energy Environ. Sci.* **2009**, *2*, 559–588.
5. Nozik, A. J. Quantum Dot Solar Cells. *Phys. E* **2002**, *14*, 115–120.
6. Kamat, P. V. Quantum Dot Solar Cells. Semiconductor Nanocrystals as Light Harvestors. *J. Phys. Chem. B* **2008**, *113*, 18737–18753.
7. Tisdale, W. A.; Williams, K. J.; Timp, B. A.; Norris, D. J.; Aydil, E. S.; Zhu, X.-Y. Hot Electron Injection from Semiconductor Nanocrystals. *Science* **2010**, *328*, 1543–1547.
8. Bockelmann, U.; Bastard, G. Phonon Scattering and Energy Relaxation in Two-, One-, and Zero-Dimensional Electron Gases. *Phys. Rev. B* **1990**, *42*, 8947–8951.
9. Gfroerer, T. H.; Sturge, M. D.; Kash, K.; Yater, J. A.; Plaut, A. S.; Lin, P. S. D.; Florez, L. T.; Harbison, J. P.; Das, S. R.; Lebrun, L. Slow Relaxation of Excited States in Strain-Induced Quantum Dots. *Phys. Rev. B* **1996**, *53*, 16474.
10. Cho, B.; Peters, W. K.; Hill, R. J.; Courtney, T. L.; Jonas, D. M. Bulk-like Hot Carrier Dynamics in Lead Sulfide Quantum Dots. *Nano Lett.* **2010**, *10*, 2498–2505.
11. Miaja-Avila, L.; Tritsch, J. R.; Wolcott, A.; Chan, W.-L.; Nelson, C. A.; Zhu, X.-Y. Direct Mapping of Hot Electron Relaxation and Multiexciton Generation Dynamics in PbSe Quantum Dots. *Nano Lett.* **2012**, *12*, 1588–1591.
12. Pandey, A.; Guyot-Sionnest, P. Slow Electron Cooling in Colloidal Quantum Dots. *Science* **2008**, *322*, 929–932.
13. Woggon, U.; Giessen, H.; Gindele, F.; Wind, O.; Fluegel, B.; Peyghambarian, N. Ultrafast Energy Relaxation in Quantum Dots. *Phys. Rev. B* **1996**, *54*, 17681–17690.
14. Klimov, V. I.; McBranch, D. W.; Leatherdale, C. A.; Bawendi, M. G. Electron and Hole Relaxation Pathways in Semiconductor Quantum Dots. *Phys. Rev. B* **1999**, *60*, 13740–13749.
15. Burda, C.; Link, S.; Mohamed, M.; El-Sayed, M. The Relaxation Pathways of CdSe Nanoparticles Monitored with Femtosecond Time-Resolution from the Visible to the IR: Assignment of the Transient Features by Carrier Quenching. *J. Phys. Chem. B* **2001**, *105*, 12286–12292.
16. Harbold, J. M.; Du, H.; Krauss, T. D.; Cho, K.-S.; Murray, C. B.; Wise, F. W. Time-Resolved Intraband Relaxation of Strongly Confined Electrons and Holes in Colloidal PbSe Nanocrystals. *Phys. Rev. B* **2005**, *72*, 195312.
17. Schaller, R. D.; Pietryga, J. M.; Goupalov, S. V.; Petruska, M. A.; Ivanov, S. A.; Klimov, V. I. Breaking the Phonon Bottleneck in Semiconductor Nanocrystals *via* Multiphonon Emission Induced by Intrinsic Nonadiabatic Interactions. *Phys. Rev. Lett.* **2005**, *95*, 196401.
18. Bonati, C.; Cannizzo, A.; Tonti, D.; Tortschanoff, A.; Van Mourik, F.; Chergui, M. Subpicosecond Near-Infrared Fluorescence Upconversion Study of Relaxation Processes in PbSe Quantum Dots. *Phys. Rev. B* **2007**, *76*, 033304.
19. Hyeon-Deuk, K.; Prezhdo, O. V. Time-Domain *ab Initio* Study of Auger and Phonon-Assisted Auger Processes in a Semiconductor Quantum Dot. *Nano Lett.* **2011**, *11*, 1845–1850.
20. Kamat, P. V. Graphene-Based Nanoassemblies for Energy Conversion. *J. Phys. Chem. Lett.* **2011**, *2*, 242–251.

21. Feng, X.; Pisula, W.; Müllen, K. Large Polycyclic Aromatic Hydrocarbons: Synthesis and Discotic Organization. *Pure Appl. Chem.* **2009**, *81*, 2203–2224.

22. Yan, X.; Cui, X.; Li, B.; Li, L.-S. Large, Solution-Processable Graphene Quantum Dots as Light Absorbers for Photovoltaics. *Nano Lett.* **2010**, *10*, 1869–1873.

23. Mueller, M. L.; Yan, X.; Dragnea, B.; Li, L.-S. Slow Hot-Carrier Relaxation in Colloidal Graphene Quantum Dots. *Nano Lett.* **2011**, *11*, 56–60.

24. Avouris, Ph. Graphene: Electronic and Photonic Properties and Devices. *Nano Lett.* **2010**, *10*, 4285–4294.

25. Castro-Neto, A. H.; Guinea, F.; Peres, N. M. R.; Novoselov, K. S.; Geim, A. K. The Electronic Properties of Graphene. *Rev. Mod. Phys.* **2009**, *81*, 109–162.

26. Dawlaty, J. M.; Shivaraman, S.; Chandrashekhar, M.; Rana, F.; Spencer, M. G. Measurement of Ultrafast Carrier Dynamics in Epitaxial Graphene. *Appl. Phys. Lett.* **2008**, *92*, 042116.

27. Sun, D.; W., Z.-K.; Divin, C.; Li, X.; Berger, C.; de Heer, W. A.; First, P. N.; Norris, T. B. Ultrafast Relaxation of Excited Dirac Fermions in Epitaxial Graphene Using Optical Differential Transmission Spectroscopy. *Phys. Rev. Lett.* **2008**, *101*, 157402.

28. George, P. A.; Strait, J.; Dawlaty, J.; Shivaraman, S.; Chandrashekhar, M.; Rana, F.; Spencer, M. G. Ultrafast Optical-Pump Terahertz-Probe Spectroscopy of the Carrier Relaxation and Recombination Dynamics in Epitaxial Graphene. *Nano Lett.* **2008**, *8*, 4248–4251.

29. Newson, R. W.; Dean, J.; Schmidt, B.; van Driel, H. M. Ultrafast Carrier Kinetics in Exfoliated Graphene and Thin Graphite Films. *Opt. Express* **2009**, *17*, 2326–2333.

30. Liu, W.-T.; Wu, S. W.; Schuck, P. J.; Salmeron, M.; Shen, Y. R.; Wang, F. Nonlinear Broadband Photoluminescence of Graphene Induced by Femtosecond Laser Irradiation. *Phys. Rev. B* **2010**, *82*, 081408(R).

31. Berciaud, S.; Han, M. Y.; Mak, K. F.; Brus, L. E.; Kim, P.; Heinz, T. F. Electron and Optical Phonon Temperatures in Electrically Biased Graphene. *Phys. Rev. Lett.* **2010**, *104*, 227401.

32. Hamilton, I. P.; Li, B.; Yan, X.; Li, L.-S. Alignment of Colloidal Graphene Quantum Dots on Polar Surfaces. *Nano Lett.* **2011**, *11*, 1524–1529.

33. Borodin, A.; Reichling, M. Characterizing TiO_2(110) Surface States by Their Work Function. *Phys. Chem. Chem. Phys.* **2011**, *13*, 15442–15447.

34. Yan, X.; Li, B.; Cui, X.; Wei, Q.; Tajima, K.; Li, L.-S. Independent Tuning of the Band Gap and Redox Potential of Graphene Quantum Dots. *J. Phys. Chem. Lett.* **2011**, *2*, 1119–1124.

35. Deskins, N. A.; Dupuis, M. Electron Transport *via* Polaron Hopping in Bulk TiO_2: A Density Functional Theory Characterization. *Phys. Rev. B* **2007**, *75*, 195212.

36. Lee, C. H.; Chang, R. K.; Bloembergen, N. Nonlinear Electroreflectance in Silicon and Silver. *Phys. Rev. Lett.* **1967**, *18*, 167–170.

37. Qi, J.; Yeganeh, M. S.; Koltover, I.; Yodh, A. G.; Theis, W. M. Depletion-Electric-Field-Induced Changes in Second-Harmonic Generation from GaAs. *Phys. Rev. Lett.* **1993**, *71*, 633–636.

38. Zhao, X. L.; Ong, S. W.; Wang, H. F.; Eisenthal, K. B. New Method for Determining Surface pK_a Using Second Harmonic Generation. *Chem. Phys. Lett.* **1993**, *214*, 203–207.

39. Kaake, L.; Jailaubekov, A.; Williams, K. J.; Zhu, X.-Y. Probing Ultrafast Charge Separation at Organic Donor/Acceptor Interfaces by a Femtosecond Electric Field Meter. *Appl. Phys. Lett.* **2011**, *99*, 083307.

40. Asbury, J. B.; Hao, E.; Wang, Y.; Ghosh, H. N.; Lian, T. Ultrafast Electron Transfer Dynamics from Molecular Adsorbates to Semiconductor Nanocrystalline Thin Films. *J. Phys. Chem. B* **2001**, *105*, 4545–4557.

41. Yan, X.; Li, B.; Li, L.-S. Colloidal Graphene Quantum Dots with Well-Defined Structures. *Acc. Chem. Res.* DOI: 10.1021/ar300137p.

42. Hendry, E.; Wang, F.; Shan, J.; Heinz, T. F.; Bonn, M. Electron Transport in TiO_2 Probed by THz Time-Domain Spectroscopy. *Phys. Rev. B* **2004**, *69*, 081101.

43. Zhu, X.-Y.; Yang, Q.; Muntwiler, M. Charge Transfer Excitons at Organic Semiconductor Surfaces and Interfaces. *Acc. Chem. Res.* **2009**, *42*, 1779–1787.

44. Long, R.; Prezhdo, O. V. *Ab Initio* Nonadiabatic Molecular Dynamics of the Ultrafast Electron Injection from a PbSe Quantum Dot into the TiO_2 Surface. *J. Am. Chem. Soc.* **2011**, *133*, 19240–19249.

45. Long, R.; English, N. J.; Prezhdo, O. V. Photo-Induced Charge Separation Across the Graphene–TiO_2 Interface Is Faster Than Energy Losses: A Time-Domain *ab Initio* Analysis. *J. Am. Chem. Soc.* **2012**, *134*, 14238–14248.

46. Manga, K. K.; Zhou, Y.; Yan, Y.; Loh, K. P. Multilayer Hybrid Films Consisting of Alternating Graphene and Titania Nanosheets with Ultrafast Electron Transfer and Photoconversion Properties. *Adv. Funct. Mater.* **2009**, *19*, 3638–3643.

47. Lu, D. Y. F.; Choi, J.; Nelson, J.; Yang, O. B.; Parkinson, B. A. Adsorption, Desorption, and Sensitization of Low-Index Anatase and Rutile Surfaces by the Ruthenium Complex Dye N3. *J. Electrochem. Soc.* **2006**, *153*, E131.